A 200 MHz Compact Environmentally-Stable Mode-Locked Figure-9 Fiber Laser

Qinghui Deng ⓘ, Ke Yin, Jianghua Zhang, Xin Zheng, and Tian Jiang ⓘ

Abstract—A compact environmentally-stable mode-locked figure-9 fiber laser is reported in this paper. The laser cavity is composed of only two all-polarization-maintaining fiber components, which enjoys a concise and stable structure. As a result, vibration-immune stable fundamental single-pulse mode-locking operation can always be observed. The pulse repetition rate was measured to be 201.14 MHz which was much higher than the most of previous works. The output pulse was also measured to have a center wavelength/3-dB spectral bandwidth/radio frequency signal to noise ratio/pulse width of 1561.29 nm/20.97 nm/78 dB/510 fs, respectively. Besides, a temperature test in the range of 20 to 36 °C, together with a 12-h output performance test was explored. The measured evolutions of output power, repetition frequency, and spectrum showed the laser had excellent environmental stability, illustrating it as an easy-fabrication, environmentally-stable and compact ultrafast candidate for the scientific area of this kind.

Index Terms—Fiber laser, laser mode locking, ultrafast fiber laser, polarization-maintaining.

I. INTRODUCTION

OVER the recent decades, ultrafast mode-locked fiber lasers [1], [2] delivering ultrashort pulses have been widely applied to abundant fields, such as optical frequency comb generation [3], optical frequency division [4], nonlinear optics [5], molecular spectroscopy [6] and confocal microscopy [7]. With the development of technology, more and more applications require pulse sources to work in unstable, even harsh environments, such as industrial workshops, submarines, and even spacecraft. The developing trend has put a critical requirement on compactness, cost efficiency and stable performance of lasers. By contrast, fiber lasers have inherent novel features including simpler structure, less space usage, and lighter weight [8], [9].

Therefore, it is a promising pulse source for operations outside the laboratory.

There are mainly two directions that researchers are trying to improve the performance of fiber lasers: one is to control parameters from the outside; the other is to improve the pulse generation mechanism. Controlling the external environment of the laser is the former, specifically placing the laser in a thermotank or a well-controlled room. However, it must be carefully controlled to ensured that the exterior remains unchanged [10]–[13]. Additionally, a phase-locking system can stabilize the pulse source parameters, and excellent performance can be obtained [14]–[16]. In this way, many stabilized fiber lasers applied outside the laboratory have been reported [17]–[20]. Nonetheless, the complex construction of the phase-locking system limits the practicability of fiber lasers.

In addition to external control, many related works dedicated improving the inherent performance of the laser has been carried out. Compared with real saturable absorbers (SAs) [21]–[24], which often deteriorate due to long-term work, the equivalent SAs based on the nonlinear effect of the cavity have the advantages of high damage threshold, ultrafast recovery time, and high cost-effectiveness. As a common equivalent SA, nonlinear polarization evolution (NPE) [25]–[27] has proven to be a promising pulse generation mechanism owing to its wavelength insensitivity. However, it is somewhat sensitive to environmental variations such as temperature, which limits its application in harsh conditions. Typically, polarization-maintaining (PM) fibers used in lasers can improve the ability of the laser to resist environmental interference. Unfortunately, NPE technology cannot be combined with PM fibers because it relies on polarization changes to achieve mode-locking.

Nonlinear amplification loop mirror (NALM) [28]–[30] is another kind of equivalent SAs used to realize passively mode-locked fiber lasers. Like NPE, it is insensitive to wavelength. More preferably, it can be combined with PM fibers to form a full PM structure. Therefore, NALM is a very promising solution for generating environmentally stable pulse sources. But the difficulty of self-starting should be considered [11], [31]. Meanwhile, a segment of long fiber is required to accumulate enough nonlinear phase shift, unfortunately, which makes the pulse repetition rate low. Hänsel *et al.* reported a novel architecture of mode-locked fiber laser, named figure-9 to distinguish it from the traditional figure-8 fiber laser [32]. Due to a nonreciprocal phase shift, the loop mirror can work in a compact and efficient reflection mode, providing the possibility of high repetition frequency. Robust work achieved a wide range
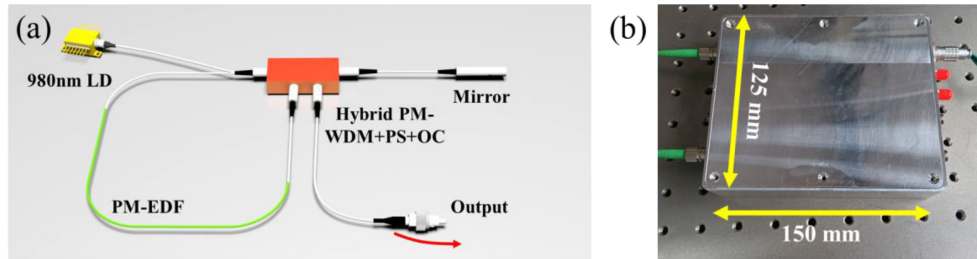
Fig. 1. (a) Schematic diagram of the 200 MHz compact mode-locked fiber laser. LD: laser diode, PM-EDF: polarization-maintaining Er-doped fiber, WDM: wavelength division multiplexer, PS: phase shifter, OC: optical coupler with the splitting ratio of 40:60. (b) Photograph of the laser package.

of 10–250 MHz repetition rate. Then, Liu *et al.* used a similar structure to obtain a robust 700 MHz mode-locked Yb:fiber laser, which greatly expanded the application range of NALM fiber lasers [33]. However, discrete or space devices were used, making the structure of these fiber lasers somewhat complex and requiring high-precision alignments [18], [20]. Thus, an all-fiber structured mode-locked figure-9 laser is desired nowadays [32].

In this paper, a 201.14 MHz environmentally-stable mode-locked fiber laser is demonstrated. By introducing a nonreciprocal phase shifter, stable mode-locking operation can always be observed in a single pulse state. Typically, the laser cavity is a figure-9 fiber cavity composed of only two all-PM fiber components: one is a homemade hybrid component and the other is a reflector. Consequently, the high repetition rate of 201.14 MHz was obtained by shortening the laser cavity length. Additionally, it was also demonstrated the repetition rate can be tuned in the range of tens of kHz through thermal tuning. And a 12-h test was explored to demonstrate the stability of Er-doped fiber laser.

II. EXPERIMENTAL SETUP

Fig. 1(a) shows the schematic diagram of the compact mode-locked figure-9 fiber laser. The overall cavity structure is simple and compact, consisting of a NALM loop, a linear reflection cavity, and a 980-nm laser diode (LD). The NALM loop is composed of a segment of 31-cm PM Er-doped fiber (PM-EDF), with gain of 80-dB/m at 1530 nm, and a homemade hybrid component.

Detailly, the hybrid component includes a wavelength division multiplexing coupler (WDM, 980 nm/1550 nm), a nonreciprocal phase shifter (PS) and a 2×2 PM optical coupler (OC) with the splitting ratio of 40:60. In the figure-9 laser, a nonreciprocal PS is essential to mode-lock because the cavity loss of continuous-light is smaller than the mode-locked state [32]. Phase shift could be provided by the PS to move the nonlinear transmission of NALM to the peak power sensitive area. Consequently, stable mode-locked operations can always be realized. Packaging multiple devices into the hybrid device makes the cavity structure simpler and more compact, which is more conducive to the widespread application of the laser. Note that the second-order dispersion of the Er-doped fiber is $6 \text{ ps}^2/\text{km}$ and that of the remaining fibers is $-22 \text{ ps}^2/\text{km}$ the calculated total dispersion is approximately -0.0124 ps^2.

The reflection cavity consists of a reflection mirror (with a reflectivity of 99%) and a 10-cm length of PM standard single mode fiber. Thus, the pulses from NALM loop are reflected by this mirror and back to the NALM loop through the OC in the hybrid component. The PM-EDF is pumped at 980 nm by the LD through WDM. In other words, the whole cavity consists of only the homemade hybrid component, the mirror and some fibers. And since the Er-fiber and passive fibers are all PM fibers, the laser oscillator is insensitive to the environmental vibrations.

In order to efficient thermal stabilization and convenient tuning, the laser is mounted in a double-layer aluminum box with the laser cavity on the upper layer and a heating plate for uniformly heating on the lower layer. Fig. 1(b) shows the photo of the whole system (the oscillator with thermal controller) in the box with a size of $125 \times 150 \times 30 \text{ mm}^3$. The right side is the input and output of the thermal controller, and the left side is the input of the system's pump light and the output of the pulsed laser.

In the experiment, the temporal property and RF spectra were performed by a 1 GHz oscilloscope with a high-speed InGaAs photodetector. The pulse width was measured with a commercial second harmonic generation based pulse autocorrelator. The optical spectrum of the mode-locked laser was recorded by an optical spectrum analyzer with a resolution of 0.02 nm. The tuning and recording of temperature could be realized by a computer. Other measuring equipment included a power meter and a frequency counter.

III. EXPERIMENTAL RESULTS

Due to the high start-up threshold of the mode-locked lasing, stable mode-locking operation was obtained when the pump power was set to the maximum value of 850 mW. After the mode-locking operation was observed, the pump power could be reduced to 190 mW, and the mode-locked state could still be achieved. In other words, the range of pump power used to achieve the mode-locked state is from 190 mW to 850 mW. However, when the pump power was greater than 300 mW, a spectral-narrow continuous lasing can be observed from the spectrum. Fig. 2(a) shows the variation of the output power with respect to the pump power. Obviously, there is a linear relationship between the two.

In the experiments, the laser repetition frequency also changed with the increase of the pump power. Fig. 2(b) shows that the
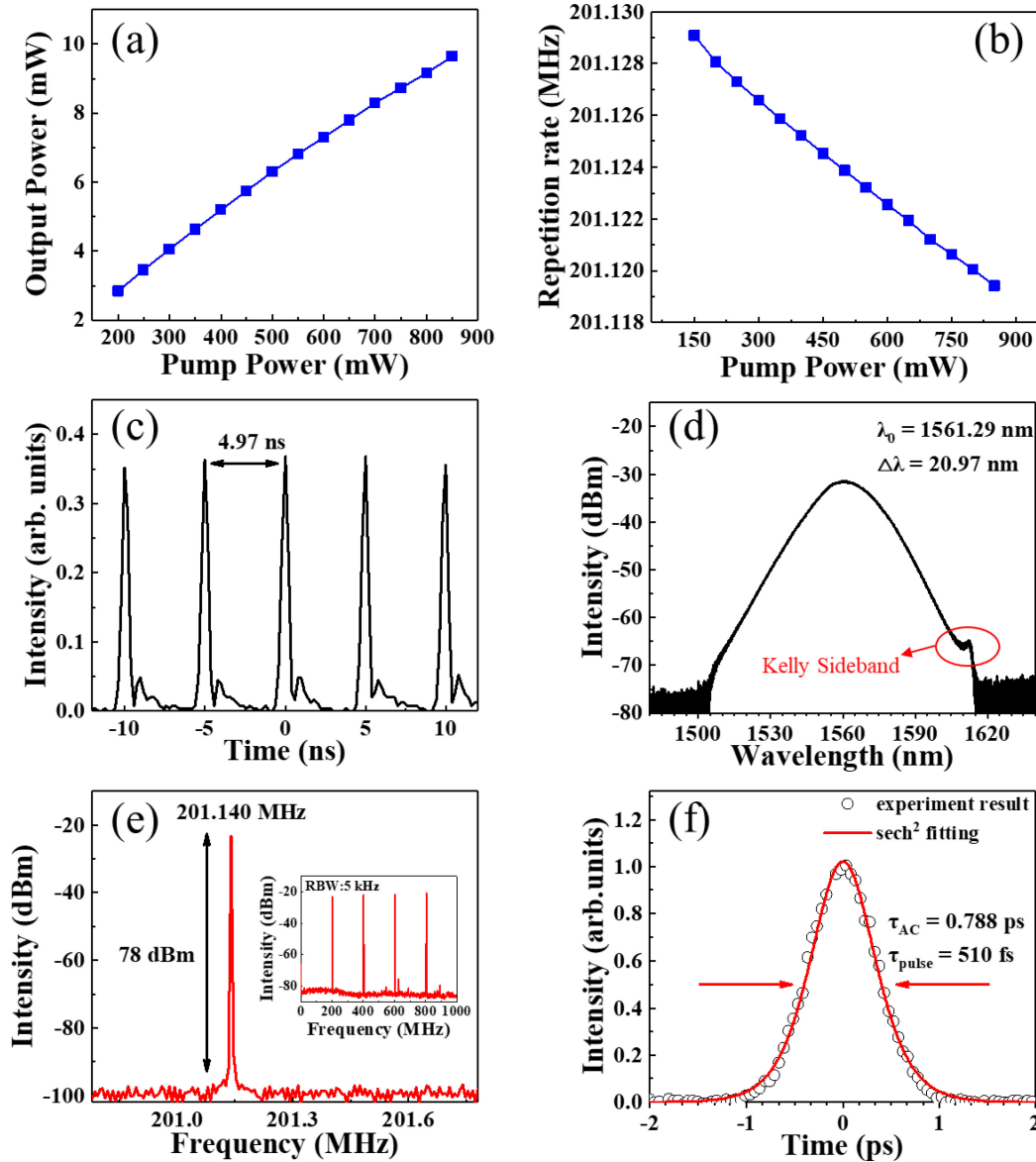
Fig. 2. Output characterization of the laser. (a) The change of the output average power under different pump power. (b) The tunable repetition rate with pump power. (c) The time-domain pulses by photodetector. (d) The optical spectrum measured with 0.02 nm resolution. (e) The measured RF spectrum showing the first harmonic and the RF spectrum in the 1 GHz range shown in the inset. (d) The pulse autocorrelation trace.

repetition rate decreases linearly with the increase of pump power, which is consistent with the description in Ref. [34]. This change of repetition frequency is caused by the interaction of self-steepening effect, intensity-dependent spectral shift, and resonance group velocity. Therefore, while the pump power is adjusted to control the carrier envelope offset frequency, the influence of the pump power for the repetition frequency should be considered.

The output characteristics of the laser were characterized at the room temperature of about 20 °C. Fig. 2(c) shows the pulses measured by a photodetector. The pulse interval is 4.97 ns, which corresponds to a round-trip time of ∼1.02 m cavity length. As shown in Fig. 2(d), the output laser has a smooth spectrum with a 3-dB spectral bandwidth of 20.97 nm centered at 1561.29 nm with a resolution of 0.02 nm, which is equivalent

to a transform-limited pulse width of ∼123 fs. In the optical spectrum, there is a Kelly sideband near 1611 nm, while the corresponding Kelly sideband on the short wavelength side is not observed. The reason for this is the short sideband was absorbed by the gain fiber because the highly absorption of the gain fiber (∼80 dB/m at 1530 nm).

In previous work, the pulse repetition rate of ∼121 MHz by cutting the intra-cavity pigtails of components could be achieved [11]. In this letter, the high repetition rate of 201.14 MHz was obtained with the homemade hybrid component and short-length intra-cavity pigtails. The measured RF spectrum is plotted in Fig. 2(e) with RBW of 30 Hz. The signal to noise ratio (SNR) of the fundamental frequency reaches 78 dBm. At the same time, the RF spectrum in the 1 GHz range was also measured, and the result is shown in the inset of Fig. 2(e). Limited by the
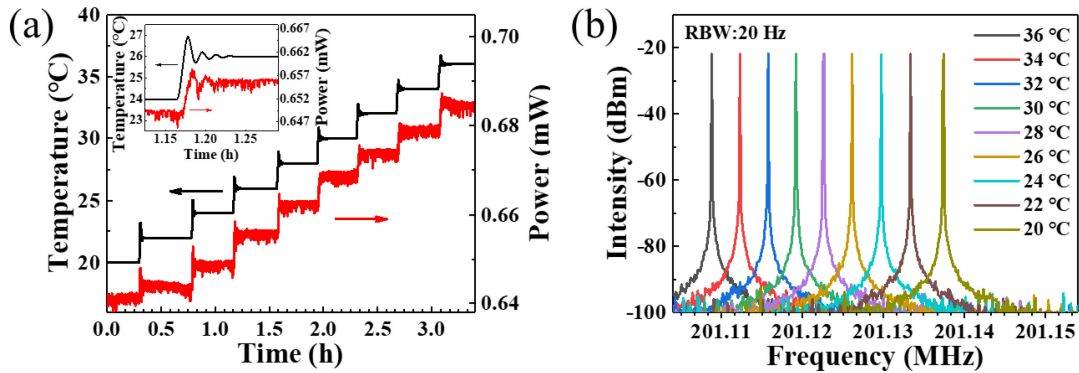
Fig. 3. During thermal tuning (a) the change of output optical power (b) the change of repetition frequency. The inset shows a zoom-in plot of the change from 24 to 26 °C.
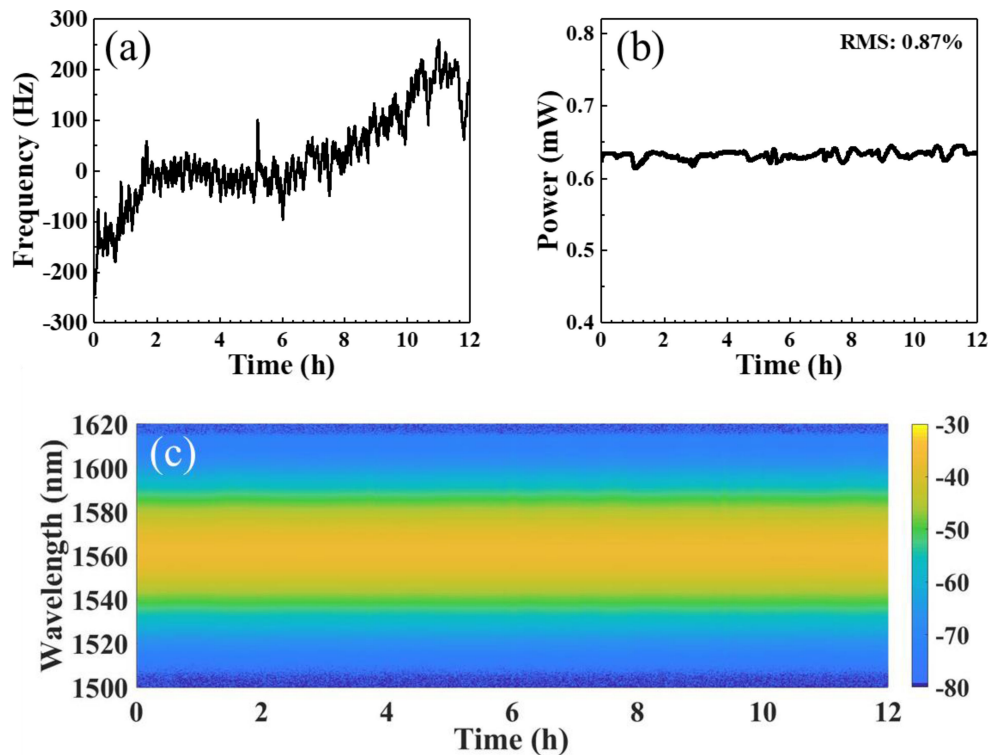

Fig. 4. 12-h measurement of the output show, showing (a) pulse repetition rate, (b) monitored optical power (1/4 of the output power), and (c) optical spectrum, where color bar represents the relative spectrum intensity in units of dBm.

bandwidth of the radio frequency instrument, the 4th harmonic was measured at most. Fig. 2(f) depicts the output autocorrelation (AC) trace after an isolator. Fitting by the AC trace with a sech^2 function, the pulse width is estimated to be $0.648 \times 0.788 \text{ ps} = 510 \text{ fs}$. This result is larger than the previously calculated pulse width $\sim$123 fs, and the corresponding time bandwidth product is calculated to be 1.315. Therefore, the output pulse has a slight chirp that can be eliminated by dispersion compensation fibers to compress the pulse width.

After the laser was placed in a double-layer aluminum box with thermal controller, the whole system can achieve efficient thermal stabilization and tuning. Benefiting from the all-fiber and PM configuration, the laser can always maintain the mode-locked state during temperature tuning. A 20–36 °C temperature

test was carried out with thermal controller. The results are shown in Fig. 3. As shown in Fig. 3(a), the mean output power is 0.66 mW (1/4 of the output power) with a fluctuation of about 45 μW, indicating a good power and mode-locking stability of the laser under the circumstance of severe temperature changing. Furthermore, in the process of temperature change in a step of 2 °C, output power changed together with the temperature, which is obvious in the illustration. There is an overshoot phenomenon in thermal tuning, as well as a slightly delay of the output power, showing that when the laser is placed in a constant temperature environment, more excellent stable performance can be obtained. Fig. 3(b) shows that the repetition rate can be widely tuned by thermal controller: by changing the temperature of the laser from 20 to 36 °C the repetition rate decreases

by 28.7 kHz, corresponding to a thermal tuning coefficient of -1.8 kHz/ °C.

Moreover, a 12 h long-term output test was carried out by placing the laser in a laboratory controlled by ordinary air-conditioning. In the meantime, the thermal controller was turned off. The results are presented in Fig. 4, showing 12-h changes of pulse repetition rate, monitored optical power (1/4 of the output power), and optical spectrum. Fig. 4(a) shows the ∼400 Hz frequency drift of pulse repetition rate. As shown in Fig. 4(b), a 0.87% relative rms fluctuation with respect to the average signal power represents that the output power of the free-running ultrafast laser is stable overall. Fig. 4(c) shows the evolution of the laser spectrum recorded in steps of 1 minute. Obviously, no center wavelength shift and any degradation in the shape of the output spectrum are observed. These results show that the laser still has excellent environmental stability even without thermal stabilization.

IV. CONCLUSION

In summary, an environmentally-stable and compact mode-locked figure-9 fiber laser is demonstrated in this paper. The stable mode-locking operation could be achieved, and the variation of the output optical power and the pump optical power has been studied. The laser cavity is composed of only two all-PM fiber components, making the cavity simple and compact. The homemade hybrid component was added into the cavity, and the high repetition rate of 201.14 MHz was obtained. Additionally, the repetition rate could be tuned in the range of tens of kHz through thermal tuning. Furthermore, the excellent stability of the laser has also been proven through a long-term test and a 20–36 °C temperature test limited by the temperature controller. It is believed that the compact, stable, high-repetition frequency laser proposed in this paper has great potential and can become a good ultrafast laser source in the fields of precision measurement, optical sensing, and light-wave microwave.

REFERENCES

[1] T. Jiang *et al.*, "Ultrafast fiber lasers mode-locked by two-dimensional materials: Review and prospect," *Photon. Res.,* vol. 8, no. 1, pp. 78–90, 2020.

[2] X. Wang *et al.*, "Program-controlled single soliton microcomb source," *Photon. Res.,* vol. 9, no. 1, pp. 66–72, 2021.

[3] Z. Zhu *et al.*, "Tunable optical frequency comb from a compact and robust Er:Fiber laser," *High Power Laser Sci. Eng.,* vol. 8, no. 17, pp. 56–61, 2020.

[4] F. Quinlan *et al.*, "Ultralow phase noise microwave generation with an Er:Fiber-based optical frequency divider," *Opt. Lett.,* vol. 36, no. 16, pp. 3260–3262, 2011.

[5] D. M. B. Lesko, H. Timmers, S. Xing, A. Kowligy, A. J. Lind, and S. A. Diddams, "A six-octave optical frequency comb from a scalable few-cycle erbium fibre laser," *Nature Photon.,* vol. 15, no. 4, pp. 281–286, 2021.

[6] A. Ozawa and T. Udem, "Very large bandwidth lasers," *Nature Photon.,* vol. 15, no. 4, pp. 247–249, 2021.

[7] E. Hase *et al.*, "Scan-less confocal phase imaging based on dual-comb microscopy," *Optica,* vol. 5, no. 5, pp. 634–643, 2018.

[8] J. Wang *et al.*, "Generation of few-cycle pulses from a mode-locked Tm-doped fiber laser," *Opt. Lett.,* vol. 46, no. 10, pp. 2445–2448, 2021.

[9] C. Ma, A. Khanolkar, Y. Zang, and A. Chong, "Ultrabroadband, few-cycle pulses directly from a mamyshev fiber oscillator," *Photon. Res.,* vol. 8, no. 1, pp. 65–69, 2020.

[10] A. Głuszek *et al.*, "Compact mode-locked Er-doped fiber laser for broad-band cavity-enhanced spectroscopy," *Appl. Phys. B,* vol. 126, no. 8, 2020, Art. no. 137.

[11] K. Yin, Y.-M. Li, Y.-B. Wang, X. Zheng, and T. Jiang, "Self-starting all-fiber PM Er:Laser mode locked by a biased nonlinear amplifying loop mirror," *Chin. Phys. B,* vol. 28, no. 12, 2019, Art. no. 124203.

[12] L. C. Sinclair *et al.*, "Invited article: A compact optically coherent fiber frequency comb," *Rev. Sci. Instruments,* vol. 86, no. 8, 2015, Art. no. 081301.

[13] D. Kim, N. H. Park, H. Lee, J. Lee, D.-I. Yeom, and J. Kim, "Graphene-based saturable absorber and mode-locked laser behaviors under gamma-ray radiation," *Photon. Res.,* vol. 7, no. 7, pp. 742–747, 2019.

[14] G. W. Truong *et al.*, "Accurate frequency referencing for fieldable dual-comb spectroscopy," *Opt. Exp.,* vol. 24, no. 26, 2016, Art. no. 30495.

[15] H.-B. Wang, H.-N. Han, Z.-Y. Zhang, X.-D. Shao, J.-F. Zhu, and Z.-Y. Wei, "An Yb-fiber frequency comb phase-locked to microwave standard and optical reference," *Chin. Phys. B,* vol. 29, no. 3, 2020, Art. no. 030601.

[16] I. Coddington, W. Swann, and N. Newbury, "Coherent dual-comb spectroscopy at high signal-to-noise ratio," *Phys. Rev. A,* vol. 82, no. 4, pp. 043817.1–043817.13, 2010.

[17] D. I. Herman *et al.*, "Precise multispecies agricultural gas flux determined using broadband open-path dual-comb spectroscopy," *Sci. Adv.,* vol. 7, no. 14, 2021, Art. no. eabe9765.

[18] B. J. Pröbster, M. Lezius, O. Mandel, C. Braxmaier, and R. Holzwarth, "FOKUS II—Space flight of a compact and vacuum compatible dual frequency comb system," *J. Opt. Soc. Amer. B,* vol. 38, no. 3, pp. 932–939, 2021.

[19] F. R. Giorgetta, W. C. Swann, L. C. Sinclair, E. Baumann, I. Coddington, and N. R. Newbury, "Optical two-way time and frequency transfer over free space," *Nature Photon.,* vol. 7, no. 6, pp. 434–438, 2013.

[20] M. Lezius *et al.*, "Space-borne frequency comb metrology," *Optica,* vol. 3, no. 12, pp. 1381–1387, 2016.

[21] X. Li *et al.*, "Fe$_3$O$_4$ nanoparticle-enabled mode-locking in an erbium-doped fiber laser," *Front. Optoelectron.,* vol. 13, no. 2, pp. 149–155, 2020.

[22] M. Jung *et al.*, "A femtosecond pulse fiber laser at 1935 nm using a bulk-structured Bi$_2$Te$_3$ topological insulator," *Opt. Exp.,* vol. 22, no. 7, pp. 7865–7874, 2014.

[23] J. Bogusławski, G. Soboń, R. Zybała, and J. Sotor, "Towards an optimum saturable absorber for the multi-gigahertz harmonic mode locking of fiber lasers," *Photon. Res.,* vol. 7, no. 9, pp. 1094–1100, 2019.

[24] R. Miao *et al.*, "Soliton mode-locked fiber laser with high-quality MBE-grown Bi$_2$Se$_3$ film," *Chin. Opt. Lett.,* vol. 17, no. 7, 2019, Art. no. 071403.

[25] C. Li *et al.*, "1 GHz repetition rate femtosecond Yb:Fiber laser for direct generation of carrier-envelope offset frequency," *Appl. Opt.,* vol. 54, no. 28, pp. 8350–8353, 2015.

[26] G. Pu, L. Yi, L. Zhang, and W. Hu, "Intelligent programmable mode-locked fiber laser with a human-like algorithm," *Optica,* vol. 6, no. 3, pp. 362–369, 2019.

[27] A. Khanolkar, Y. Zang, and A. Chong, "Complex swift hohenberg equation dissipative soliton fiber laser," *Photon. Res.,* vol. 9, no. 6, pp. 1033–1038, 2021.

[28] A. S. Mayer *et al.*, "Flexible all-PM NALM Yb:Fiber laser design for frequency comb applications: Operation regimes and their noise properties," *Opt. Exp.,* vol. 28, no. 13, pp. 18946–18968, 2020.

[29] D. Duan, J. Wang, Y. Wu, J. Ma, and Q. Mao, "Approach to high pulse energy emission of the self-starting mode-locked figure-9 fiber laser," *Opt. Exp.,* vol. 22, pp. 33603–33613, 2020.

[30] J. Zhou, W. Pan, X. Fu, L. Zhang, and Y. Feng, "Environmentally-stable 50-fs pulse generation directly from an Er:Fiber oscillator," *Opt. Fiber Technol.,* vol. 52, pp. 101963.1–101963.5, Nov. 2019.

[31] J. Kim and Y. Song, "Ultralow-noise mode-locked fiber lasers and frequency combs: Principles, status, and applications," *Adv. Opt. Photon.,* vol. 8, no. 3, pp. 465–540, 2016.

[32] W. Hänsel *et al.*, "All polarization-maintaining fiber laser architecture for robust femtosecond pulse generation," *Appl. Phys. B,* vol. 123, no. 1, pp. 41.1–41.6, 2017.

[33] G. Liu, X. Jiang, A. Wang, G. Chang, F. Kaertner, and Z. Zhang, "Robust 700 MHz mode-locked Yb:Fiber laser with a biased nonlinear amplifying loop mirror," *Opt. Exp.,* vol. 26, no. 20, pp. 26003–26008, 2018.

[34] N. R. Newbury and B. R. Washburn, "Theory of the frequency comb output from a femtosecond fiber laser," *IEEE J. Quantum Electron.,* vol. 41, no. 11, pp. 1388–1402, 2005.